Desalination and Water Treatment 320 (2024) 100582

Contents lists available at ScienceDirect

Desalination and Water Treatment

journal homepage: www.sciencedirect.com/journal/desalination-and-water-treatment/

Application of perovskite-structured lithium titanate towards remediation of environmental pollutants

K.M. Gopalakrishnan[a], S. Nilesh[a], G. Kathiresan[a], Abhay Kumar[a], K. Vallarasu[a], R. Anitha[b], V. Vijayalakshmi[b,*]

[a] Department of Civil Engineering, Erode Sengunthar Engineering College, Erode 638057, India
[b] Department of Physics, Erode Sengunthar Engineering College, Erode 638057, India

ARTICLE INFO

Keywords:
Visible light
Methylene blue
Lithium titanate
Photocatalysis

ABSTRACT

The advancement of new materials for water treatment and environmental remediation is becoming increasingly vital in the face of growing global issues like water scarcity, pollution, and ecosystem degradation. Cutting-edge nanomaterials offer notable enhancements in efficiency, selectivity, and sustainability compared to traditional techniques. These advanced materials can effectively remove a broad spectrum of contaminants, including heavy metals, organic pollutants, and pathogens, from water sources. Additionally, they facilitate the creation of more sustainable and cost-efficient treatment processes, which are crucial for safeguarding public health and maintaining environmental quality. Ongoing developments in material science not only improve the performance of current water treatment technologies but also foster the development of new methods that can tackle emerging contaminants and adjust to various environmental conditions. This highlights the essential role of material innovation in progressing water treatment and environmental remediation technologies, emphasizing its significance in providing safe, clean water and promoting a healthier environment. For the first time, in this report we report that Sm and Ba doped $Li_4Ti_5O_{12}$ NPs for treating industrial wastewater to remove organic contaminants. The lithium titanate doped with Sr and Ba was synthesized using coprecipitation methods. The photocatalytic degradation activity of Sr/Ba/ $Li_4Ti_5O_{12}$ was significantly increased in comparison to pure $Li_4Ti_5O_{12}$, attaining 98.5 % methylene blue degradation in 100 min under visible light. By coprecipitation and calcination, highly crystalline bare and doped $Li_4Ti_5O_{12}$ NPs were effectively synthesized using lithium nitrate, titanium tetra isopropoxide, and KOH as precursors. By introducing Sr- and Ba-ion impurities to the lattice, $Li_4Ti_5O_{12}$'s electronic band structure was altered and its absorption into the visible region was increased.

1. Introduction

Ecosystems and human health are seriously threatened by dye pollution, such as that caused by methylene blue (MB). Particularly frequent pollutants like MB persist in aquatic settings because they are resistant to natural degradation mechanisms. Serious ecological harm, such as toxicity to aquatic life and interference with normal photosynthetic processes, can result from its persistence [1]. To reduce their negative effects on the environment and guarantee safety, it is crucial to create efficient processes for breaking down these dyes. In order to effectively decompose MB and related pollutants and aid in the preservation and restoration of environmental quality, cutting-edge materials and cutting-edge treatment techniques are crucial in tackling this problem. The elimination of MB from polluted water is essential due to its extensive use in various industries and its detrimental environmental effects [2]. Current technologies for removing MB include adsorption, coagulation, membrane filtration, and advanced oxidation processes. Although these methods are effective, they often face challenges such as high costs, complex operations, and the potential for secondary pollution. Photodegradation, which uses light energy to break down pollutants, has emerged as a promising alternative for dye removal. This technique is particularly appealing because of its high efficiency, environmental friendliness, and the use of renewable solar energy. In this study, photodegradation was chosen and examined for its ability to effectively degrade MB under mild conditions without producing harmful by-products. By investigating the use of advanced materials in photodegradation, this research aims to improve the efficiency and feasibility of MB removal, contributing to cleaner and safer water environments [3].

New materials for energy conversion and environmental remediation have been the focus of scientific research recently. In the realm of

---

* Corresponding author.
E-mail address: vijiphysics007@gmail.com (V. Vijayalakshmi).

https://doi.org/10.1016/j.dwt.2024.100582
Received 11 March 2024; Received in revised form 19 June 2024; Accepted 1 July 2024

photocatalysis, perovskite titanate nanoparticles have become a prominent class of materials with great potential for improving energy conversion technologies and solving environmental issues [4]. These nanoparticles have remarkable photocatalytic activity because of their distinct crystal structure, adjustable bandgap, and adaptable chemical characteristics. They are frequently based on the generic chemical formula ABO_3, where A is a cation and B is a transition metal cation [5]. The three-dimensional network of corner-sharing BO_6 octahedra encircled by A-site cations that make up the perovskite structure is perfect for photocatalytic processes. Perovskites based on titanium, in particular, have surface characteristics and advantageous electronic configurations that facilitate catalytic reactions, charge separation, and light absorption. Perovskite titanate nanoparticles have proven to be incredibly effective in a variety of photocatalytic applications, such as the production of solar fuel, water splitting, and pollutant degradation [6]. Their adaptable synthesis pathways and customizable composition provide the possibility to adjust their characteristics to meet certain environmental and catalytic needs. Among them, $Li_4Ti_5O_{12}$ NPs (Lithium titanate) are one of these materials that have attracted a lot of interest because of their special qualities and range of uses, especially in photocatalysis [7]. Utilizing light energy to propel chemical processes is known as photocatalysis, and it has great potential to address urgent environmental issues including energy conversion, air cleanup, and water purification. Owing to their strong chemical stability, large surface area, and advantageous band structure, $Li_4Ti_5O_{12}$ NPs have remarkable photocatalytic activity [8]. Because of their large bandgap and effective charge carrier separation, these nanoparticles are used for catalytic reactions across a wide range of light wavelengths. Furthermore, their nanoscale size allows for improved surface contacts, which boost catalytic kinetics and efficiency [9].

To increase semiconductor nanoparticle photocatalytic activity, we have been investigating different doping schemes, such as adding metals like barium (Ba) and strontium (Sr) to the lattice of $Li_4Ti_5O_{12}$ NPs. By purposefully altering the composition of the nanoparticles, the goal is to improve their surface, optical, and electrical characteristics, which will increase their effectiveness in photocatalytic applications [10]. Because strontium and barium have comparable chemical properties to $Li_4Ti_5O_{12}$ NPs, doping them with these metals presents interesting options for modifying the properties of the nanoparticles. Several effects, including band structure alterations, defect engineering, and increased charge carrier dynamics essential for effective photocatalysis be obtained by replacing lithium ions within the crystal lattice with Sr or Ba ions [11]. Strontium and barium doping of $Li_4Ti_5O_{12}$ NPs has synergistic effects that show promise for a variety of photocatalytic applications, such as air and water cleaning and the production of renewable energy [12]. Employing methodical investigations and sophisticated material engineering, scientists want to fully utilize doped lithium titanate nanoparticles to tackle urgent environmental issues and facilitate the advancement of sustainable technology [13]. Our goal is to improve the photocatalytic efficiency of the Sm and Ba doped $Li_4Ti_5O_{12}$ semiconductor NPs and open the door for the development of the next generation of effective and adaptable photocatalysts by clarifying the complex relationship between dopants, structure, and photocatalytic activity.

2. Materials and methods

2.1. Chemicals

Analytical-grade Lithium Nitrate ($LiNO_3$, 98 %), Strontium Nitrate ($Sr(NO_3)_2$, 98.5 %), Barium Nitrate ($Ba(NO_3)_{2,}$ 99 %) and Pottasium Hydroxide Pellet (KOH, 85 %), along with Titanium tetra isopropoxide [$TiOCH(CH_3)_2)_4$ 97 %], were procured from Merck ltd. The chemicals were employed in their original form without additional purification. Furthermore, all aqueous solutions were prepared using deionized water.

2.2. SYNTHESIS OF $Li_4Ti_5O_{12}$ and Sr, Ba, Sr/Ba doped $Li_4Ti_5O_{12}$ samples

In a sterile beaker designated solution A, combine 50 ml of DD water with 3.447 g of $LiNO_3$. Place 5.7 ml of TTIP and 20 ml of propanol in a different beaker labelled solution B. Stir the mixture thoroughly for thirty minutes. Next, combine solution A with solution B. Then, 5.61 g of KOH was added to the mixture above after 30 min. The aforementioned combination was then centrifuged many times using ethanol and water. Eventually, a 24-hour oven dry at 80 °C was applied to the semi-solid liquid. Use a mortar and pestle to grind the dried gel into a fine powder and calcined for two hours at 450 °C shown in Fig. 1.

To prepare Sr doped $Li_4Ti_5O_{12}$ (0.05 M Sr.), $Li_4Ti_5O_{12}$ was suspended in twice-distilled water and exposed to an ultrasound bath for 10 min. Then, strontium nitrate ($Sr(NO_3)$) was added to the suspension, and NH_4OH was added dropwise. The mixture reaction was exposed again to an ultrasound bath for 10 min. The obtained materials were filtered at vacuum, dried at 80 °C for 24 h, and calcined at 450 °C for 4 h. The same procedure was followed to prepare Ba doped $Li_4Ti_5O_{12}$ NPs. In this procedure we have used 0.05 M $Ba(NO_3)_3$ was added to the suspension, and NH_4OH was added dropwise. The mixture reaction was exposed again to an ultrasound bath for 10 min. The obtained materials were filtered at vacuum, dried at 80 °C for 24 h, and calcined at 450 °C for 4 h. Sr/Ba/ $Li_4Ti_5O_{12}$ NPs were prepared in the same manner [11].

2.3. Characterization techniques

Using an X-ray diffraction technique in the Bragg's angle range of 2θ (20–80°) and Panalytical's X′Pert PRO system, Cu Kα radiation with a wavelength = 1.5406 Å at 30 kV, USA, the structure of the produced sample and nanofiller was examined. Using a field-outflow examining electron magnifying lens (FE-SEM), the surface geology and synthesis of the nanoparticles were studied. Using a field-outflow examining electron magnifying lens (FE-SEM), the surface geology and synthesis of the nanoparticles were studied. Furthermore, FESEM, Zeiss Leo Supra 50 VP Oxford SEM, was utilized to investigate the materials' morphology and chemical composition. To examine the optical characteristics, an ultraviolet/visible spectrophotometer (UV/VIS, Systronics) was used at room temperature in the wavelength range of 190–800 nm. Decolorization through photolysis tests is conducted using a photocatalytic reactor that is constructed with a sturdy steel chamber.

2.4. Photocatalytic activity

When exposed to UV light, the breakdown of MB, the test pollutant, was measured to test and evaluate the photodegradation efficiency of the generated $Li_4Ti_5O_{12}$ NPs. At the photodegradation sample location, the Philips UV lamp produced UV light with a wavelength of 400–800 nm and an intensity of around 125 mW/cm^2 (15 W). MB dye concentration was set at 10 mg/L. The solution pH was adjusted to 7 to maintain neutrality. To achieve equal dispersion, 0.005 g of the generated samples were added to the MB solution, which was then well-mixed and sonicated. To attain adsorption-desorption equilibrium, the reaction mixture containing the MB-created samples was subsequently exposed to darkness for approximately two hours. After that, various durations of UV irradiation (0, 20, 40, 60, 80 and 100 min) were used to make sure the photocatalysts and MB solution were mixed equally. UV irradiation is used in conjunction with stirring, to ensure the photocatalysts and MB solution are well-mixed, thereby maintaining an effective suspension during photocatalytic degradation tests. The reaction mixture was centrifuged, and the photocatalysts were taken out. UV–vis absorption spectroscopy was used to measure the steady-state absorption of MB in the solution to track its concentration. Photolysis (η) is a degradation efficiency metric defined as follows:

$$\eta = \left(1 - \frac{C}{C_0}\right) \times 100\,(\%)$$

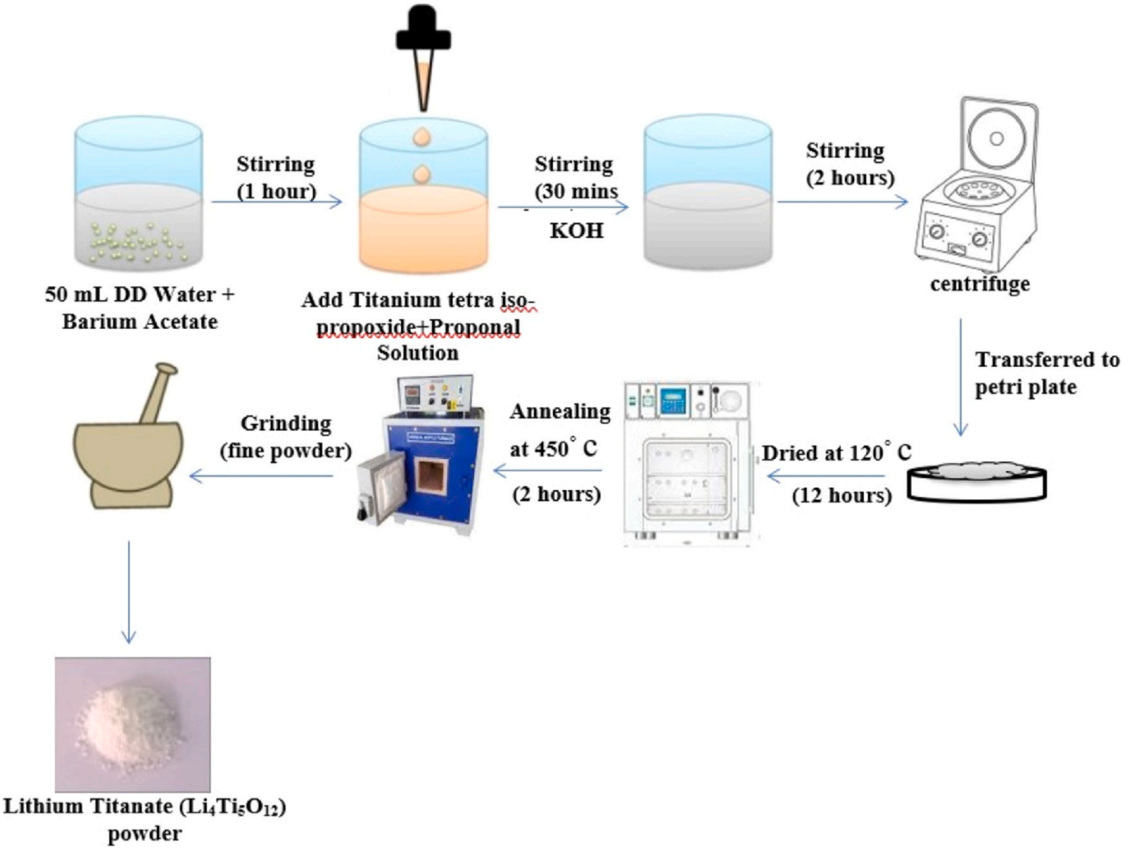

Fig. 1. Schematic Diagram of Synthesis of $Li_4Ti_5O_{12}$ NPs.

The absorbance measurement of the MB solution without catalysts is characterized by C_0 when UV irradiation is delivered after a predefined duration (t = 0), whereas the absorbance measurement of the MB solution combined with catalysts following UV treatment is characterized by C [15].

3. Result and discussion

3.1. Structural properties

The XRD spectrum of the $Li_4Ti_5O_{12}$ samples, Fig. 2 depicts the semicrystalline nature, as a result of the presence of $Li_4Ti_5O_{12}$ samples, and shows two main sharp peaks at 32.43° and 45.36°. These two peaks are attributed to planes (113) and (133) [JCPDS File No 49–0207] [16]. The remarkable crystallinity of the produced nanomaterials is demonstrated by the acute intensity of the crystal plane (1 1 3). Also, the XRD spectrum for all samples shows many low intense peaks at 2θ = 20.71°, 39.65°, 56.66° and 67.82°, corresponding to lattice planes (111), (114), (006), and (062). The obtained results verified that $Li_4Ti_5O_{12}$ has a cubic structure [9]. For the XRD of samples with Sr and Ba addition, the intensity of two main diffraction peaks decreases, and their broadness increases. Also, no new diffraction peaks are observed for doped $Li_4Ti_5O_{12}$ samples [14].

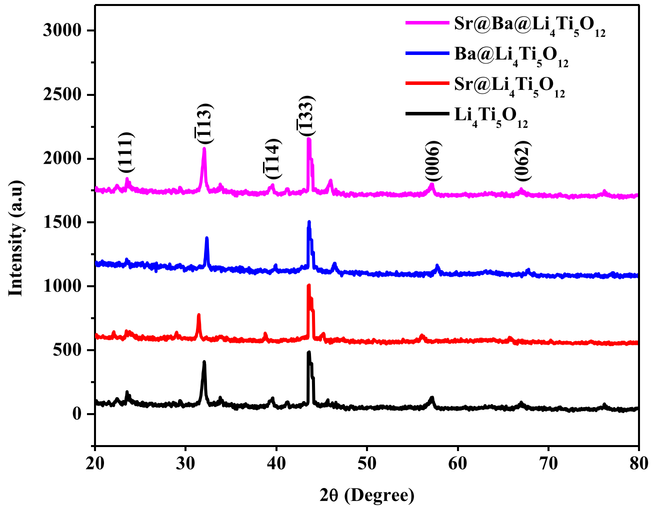

Fig. 2. XRD patterns of prepared $Li_4Ti_5O_{12}$ and Sr, Ba, Sr/Ba doped $Li_4Ti_5O_{12}$ samples.

Additionally, Scherer's equation is used to calculate the size of crystallites (D).

$$D = (0.9 \times \lambda)/(\beta \times \cos\theta)\ (\text{Å}) \tag{1}$$

Where λ is the Cu Kα 1.5406 Å wavelength, β is the FWHM (rad), and θ is the diffraction angle in degrees. The doped sample exhibited a progressive rise in average crystalline size, whereas the as-prepared sample had the lowest average crystalline size, measuring around 19, 21, 24 nm and 26 nm [17].

Fig. 3(a–d) shows the FE-SEM pictures of $Li_4Ti_5O_{12}$ and Sr, Ba, Sr/Ba doped $Li_4Ti_5O_{12}$ samples, separately, this demonstrates the aggregation of the circular molded particles with smaller crystallites and homogeneous size circulation [18]. The agglomeration of the crystallites might be attributed to the combined effects of the mixing method and Sr and Ba-particle doping. Every sample has a comparable morphology. As a result, changing the dopant concentration has no significant effect on the size and shape of the nanoparticles' surface. Pure and Sr, Ba-substituted $Li_4Ti_5O_{12}$ NPs' compound organization was determined by EDX analysis shown in Table 1, confirming the presence of dopants such as Sr and Ba in samples from different examined areas. To confirm that all parts were present in the tests under investigation, EDX calculations were performed for testing with different Sr and Ba focuses. The Ti, Sr,

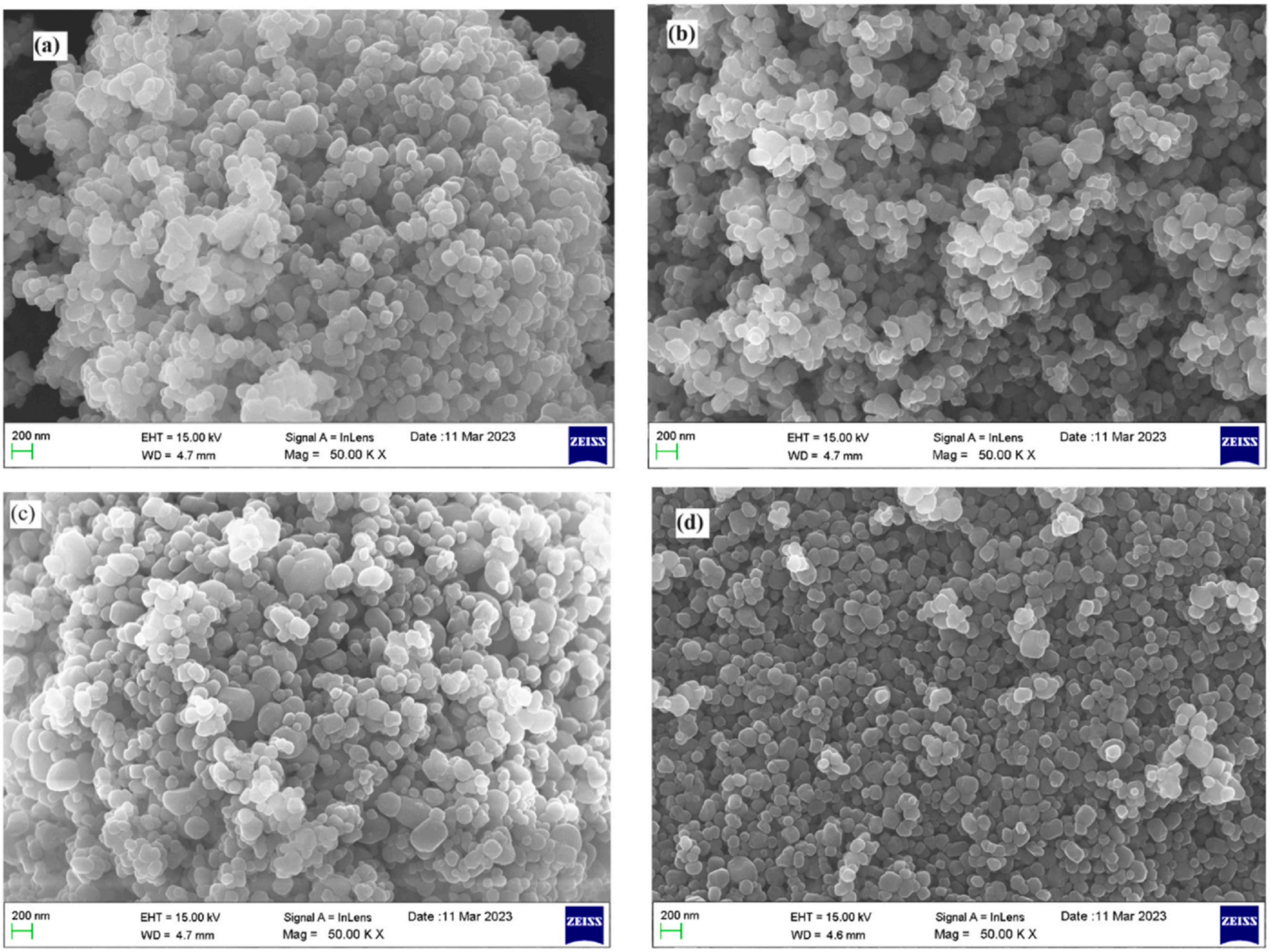

Fig. 3. Field Emission Scanning electron microscope (FESEM) images of (a-d) $Li_4Ti_5O_{12}$ and Sr, Ba, Sr/Ba doped $Li_4Ti_5O_{12}$ samples.

Table 1
Atomic percentage of undoped and Sr, Ba, Sr/Ba doped $Li_4Ti_5O_{12}$.

Doping concentrations (wt%)	Atomic ratio (at%)			
	Ti	O	Sr	Ba
Pure $Li_4Ti_5O_{12}$	19.64	78.17	-	-
Sr- $Li_4Ti_5O_{12}$	22.39	72.38	0.96	-
Ba $Li_4Ti_5O_{12}$	21.96	72.65	-	1.41
Sr/Ba/$Li_4Ti_5O_{12}$	22.61	71.06	0.79	1.01

Ba, and O components found in the samples were confirmed by the EDX findings, confirming the materials' integrity. Remaining percentage is Li ion.

Raman spectroscopy is well recognized as a very sensitive technique for examining the structural phase transition and strain signature [19] that exist in a material. The enlarged image of the chosen locations is shown in the inset of Fig. 4. The existence of strain in the samples is confirmed by a discernible shift in the Raman phonon mode's vibrational frequency [20]. It is noteworthy that the Raman spectrometer has a resolution of more than 0.5 cm^{-1}. Throughout the research, various power densities, integration durations, and settings were employed, and the overall look of the results remained relatively unchanged. The samples showed a peak in 1052 cm^{-1}, which is related to the symmetric stretch of $CaCO_3$ vibration [21]. According to reported work [22], the bands at nearly: 874, 645, 406 and 288 $cm^{-1}$are related to the tetragonal structure of lithium titanate. Since of the isotropic distribution of the electrostatic forces around the Ti^{4+} ions within each octahedron, all optical modes of $Li_4Ti_5O_{12}$ with perfect cubic symmetry should be inactive for Raman spectroscopy, according to Freire and Katiyar [22]. In Raman spectroscopy, the tetragonal and orthorhombic polars are active, and the same is true for polymorphs.

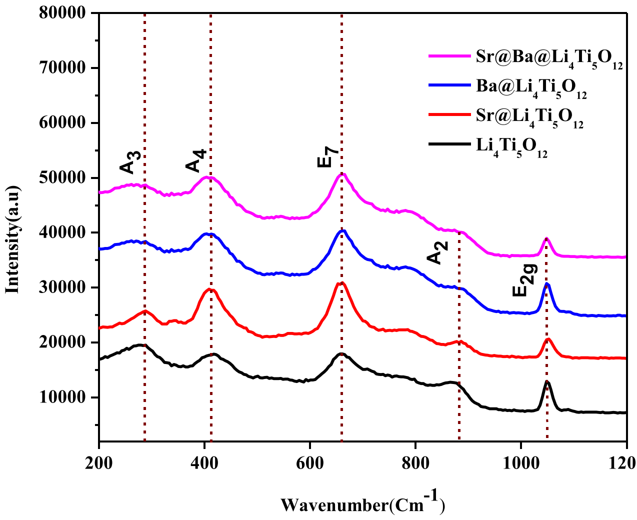

Fig. 4. RAMAN Spectrum of prepared $Li_4Ti_5O_{12}$ and Sr, Ba, Sr/Ba doped $Li_4Ti_5O_{12}$ samples.

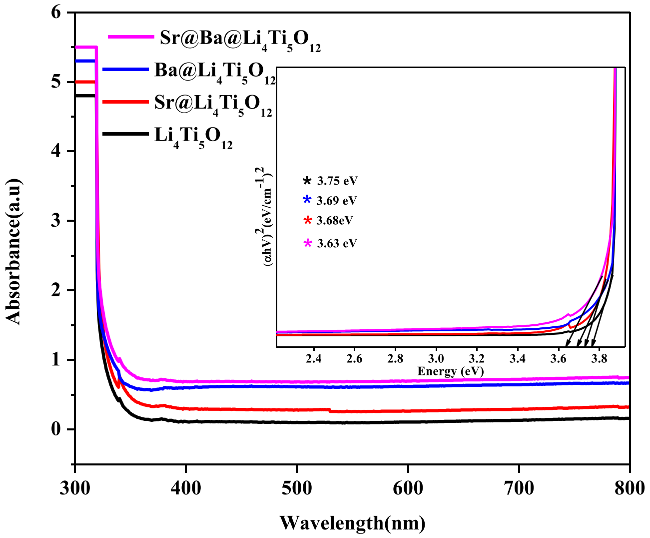

Fig. 5. The UV-Vis spectrum of $Li_4Ti_5O_{12}$ and Sr, Ba, Sr/Ba doped $Li_4Ti_5O_{12}$ samples.

3.2. UV–visible absorption studies

The UV/Vis absorbance spectra for the virgin and filled films are shown in Fig. 5. The absorbances of the samples depend on the number of constituents such as contaminations, energy holes, abandons, and rough surfaces. The transition n → π * (R band) is responsible for the tiny band observed at 331 nm in the spectra of a pure mix [23]. This band becomes much more absorbent and shifts towards longer wavelengths. Additionally, the pure blend's spectra exhibit a pronounced absorption edge that shifts towards longer wavelengths when the $Li_4Ti_5O_{12}$ inside the dopant matrix increases. This shift might be the result of complexation/homogeneity between $Li_4Ti_5O_{12}$ NPs and the dopant matrix, as well as variations in the degree of crystallinity for doped samples, which suggests variations in the optical energy gap (Eg) [11]. The following formula [6] is used to get the (Eg) value using UV/Vis absorption spectra:

$$E\,g = h\nu/\lambda = 1240/\lambda \tag{2}$$

Where ν is the speed of light, h is Planck's constant, and λ is the frequency of maximum absorption, Furthermore, using the Tauc equation and Tauc plot in addition to the band gap measurement at the wavelength of maximum absorption as shown in Eq. (3), the spectral band gap of the generated $Li_4Ti_5O_{12}$ NPs was determined and Table 2.

$$\propto h\,\nu = A\,(h\nu - Eg)\,n \tag{3}$$

Where h ν is the indicative of the incident photon energy, A and n are constants, α is the absorption coefficient and Eg is the band gap of the material. By extending the direct aspect of the $(\alpha h\nu)^2$ against hν plot to the X-axis, the Eg esteem was obtained. The material's bandgap is indicated by Fig. 5, which displays the abrupt assimilation at around 342 nm, indicating the transition from the valence band (VB) to the conduction band (CB). It is found that the energy hole of $Li_4Ti_5O_{12}$ NPs is 3.75 eV, whereas the intentional energy hole of Ba/ $Li_4Ti_5O_{12}$ is around 3.69 eV (Fig. 3). 3.68 eV and 3.63 eV are the band energy holes of Sr/ $Li_4Ti_5O_{12}$ and Ba/Sr/ $Li_4Ti_5O_{12}$ NPs respectively [24]. The drop in Eg on doped NPs was described in detail by Chun-Ming et al. [16]. The parent composite's alloying effect with certain impurity stages can be the source of the band hole shrinking [15]. Doped $Li_4Ti_5O_{12}$ NPs have a smaller energy hole than pure $Li_4Ti_5O_{12}$ NPs. The increase of contributory energy levels of Sr and Ba particles in the unique energy hole of $Li_4Ti_5O_{12}$ NPs which can be the cause of the energy hole's reduction [18].

Table 2
Band gap values for the prepared samples were computed and listed below:.

Sample	Band Gap (eV)
$Li_4Ti_5O_{12}$	3.75
Ba@ $Li_4Ti_5O_{12}$	3.69
Sr@ $Li_4Ti_5O_{12}$	3.68
Ba@Sr@$Li_4Ti_5O_{12}$	3.63

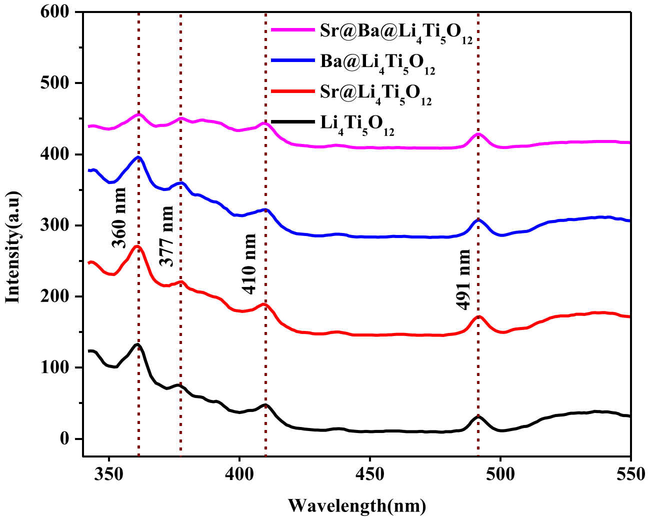

Fig. 6. PL Emission Spectra of Prepared $Li_4Ti_5O_{12}$ and Sr, Ba, Sr/Ba doped $Li_4Ti_5O_{12}$ samples.

3.3. PL emission spectrum

Photoluminescence (PL) spectra of Pure, Sr, Ba and Sr/Ba-doped $Li_4Ti_5O_{12}$ NPs are planted in Fig. 6. All the samples were energized utilizing 350 nm frequency and show the discharge groups at ∼ 360, 377, 410, and 491 nm. PL discharge band is identified with the recombination of energized electrons and gaps, so the higher PL force shows a quicker in recombination rate, which thus increments in the conductivity of the material, relating to the energy of 3.75 eV, 3.69 eV, 3.68 eV and 3.63 eV normal for surrenders on a superficial level [21]. The force of the tops at 491 nm demonstrates the Eg of the samples and it is noticed that the power is diminished with the expansion of Sr/Ba doping. In the Sr and Ba-doped $Li_4Ti_5O_{12}$ NPs, Sr^{2+} and Ba^{2+} particles substitute the Li^{4+} particles, because of their ionic sweep. The extra charge of Li position is repaid by oxygen opportunity in the cross-section. The opportunity made reason deformity levels and consequently expanded the discharge in the PL range [22].

3.4. Photocatalytic degradation of MB dye

3.4.1. Degradation efficiency and contact time

The synthesized $Li_4Ti_5O_{12}$ NPs and Sr/$Li_4Ti_5O_{12}$, Ba/ $Li_4Ti_5O_{12}$, Sr/Ba/ $Li_4Ti_5O_{12}$ materials were tested for the synergist action towards the PCD (Photocatalytic Degradation) of methylene blue (MB) under stimulated UV light illumination. The PCD tests were directed after adsorption harmony was achieved in 0–100 mins.

Fig. 7(a-d) shows the PCD of MB color regarding brightening time over various groupings of combined materials. The PCD movement of MB was not identified in the clear under stimulated UV light. The PCD action of MB arrangement utilizing Sr/Ba/ $Li_4Ti_5O_{12}$ NPs indicated preferred corruption proficiency over different samples (Fig. 10). It was discovered that the assimilation force of MB diminished with increment of time steadily. As the exposure period was increased, the primary absorption peak at 664 nm steadily shrank, signifying the photocatalytic destruction of the

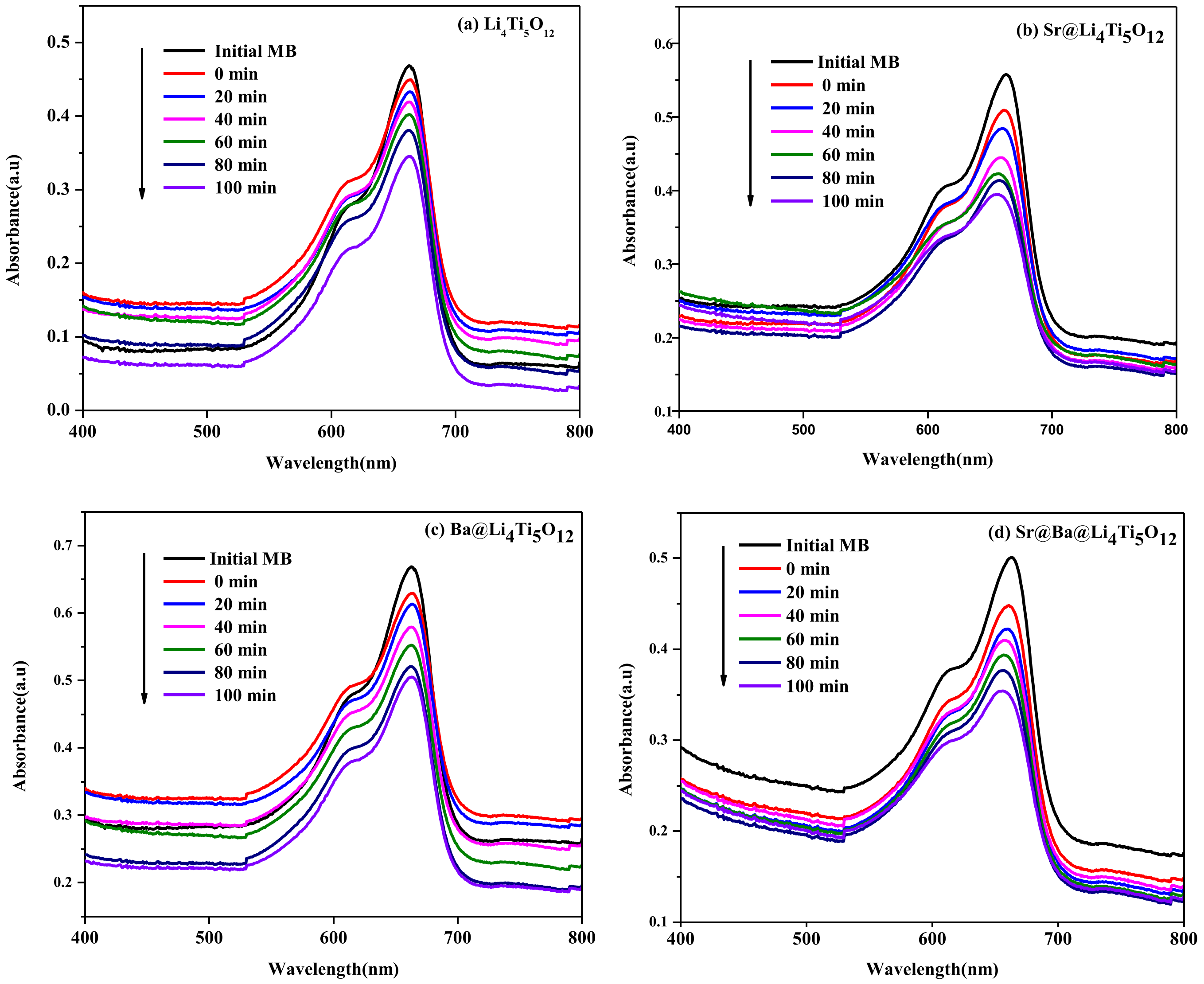

Fig. 7. (a-d). UV spectrum of MB dye degradation using for $Li_4Ti_5O_{12}$ and Sr, Ba, Sr/Ba doped $Li_4Ti_5O_{12}$ samples.

MB dye. The Sr/Ba/ $Li_4Ti_5O_{12}$ NPs higher corruption level of 98.5 % for MB. The literature on photocatalysis studies indicates that the size, shape, and crystallographic structure of the particles can all have a significant impact on photocatalytic activity [23]. As we previously indicated, enhanced optical absorption and charge carrier separation are simultaneously attributed to surface oxygen vacancies Pure, Sr, Ba, and Sr/Ba doped $Li_4Ti_5O_{12}$ nano-heterojunctions. As anticipated, Sr/Ba doped $Li_4Ti_5O_{12}$ photocatalysts demonstrated increased photocatalytic degradation efficiencies of MB from aqueous solution under simulated UV irradiation [25].

Reaction kinetic investigations of the catalyst's degradation of the methylene blue (MB) dye were described by a pseudo-first-order equation shown in Fig. 8(a-b). The equation ln $(C_0 / C) = kt$, where k and t are a pseudo-first-order kinetic constant and irradiation time. Throughout the experiment, these values are obtained at various time (t) intervals. No matter which organic pollutants, the photocatalytic activity and degradation rate of $Li_4Ti_5O_{12}$ nanoparticles go up at first and then decrease with Sr, Ba and Sr/Ba loading, with a maximum at Sr/Ba/ $Li_4Ti_5O_{12}$. Excitingly, it only took almost 100 min for Sr/Ba/ $Li_4Ti_5O_{12}$ to degrade MB under simulated UV light irradiation at room temperature (30 °C), which possesses superior photocatalytic degradation efficiency compared to the existing $Li_4Ti_5O_{12}$-based photocatalysts. The UV-induced photodegradation of MB, indicates that the UV light activities caused by the LSPR and oxygen vacancy defects play vital roles in the current system. Moreover, the photostability was evaluated by cycling experiments are as follows: After each run, the Sr/Ba/ $Li_4Ti_5O_{12}$ was recycled by a series of procedures including filtration, washing and drying, and applied for the next run [25]. The catalyst did not lose its catalytic activity for up to Four cycles and shown in Fig. 11.

3.4.2. Mechanism of decolorization

$Li_4Ti_5O_{12}$ and samples doped with Sr, Ba, and Sr/Ba were used in the photocatalytic degradation of MB dye under UV light (Fig. 7(a-d)). In the absence of light, the photocatalytic reaction of MB also occurred, resulting in reduced degradation (14 %). However, because of the tiny particle size and increased number of active sites present in Sr/Ba/ $Li_4Ti_5O_{12}$ NPs, this reaction demonstrated 98.5 % photo-decolorization of MB when exposed to UV light. Since perovskite titanate compounds can generally absorb UV light, the produced Sr/Ba/ $Li_4Ti_5O_{12}$ NPs showed better photocatalytic activity for MB degradation than other $Li_4Ti_5O_{12}$ NPs. Taking this into consideration, the likely mechanism of photocatalytic degradation processes for MB dye in the presence of $Li_4Ti_5O_{12}$ NPs is explored (Fig. 10). Redox reactions of MB dye in aqueous solution are facilitated by the $Li_4Ti_5O_{12}$ NPs photocatalysts' ability to create electron-holes (h^+) from incoming light with adequate energy. On the surface of the $Li_4Ti_5O_{12}$ photocatalyst, oxygen (O_2), water (H_2O), and dye molecules absorb. This causes holes (h^+) to be created when electrons (e^-) move from the conduction band (CB) into

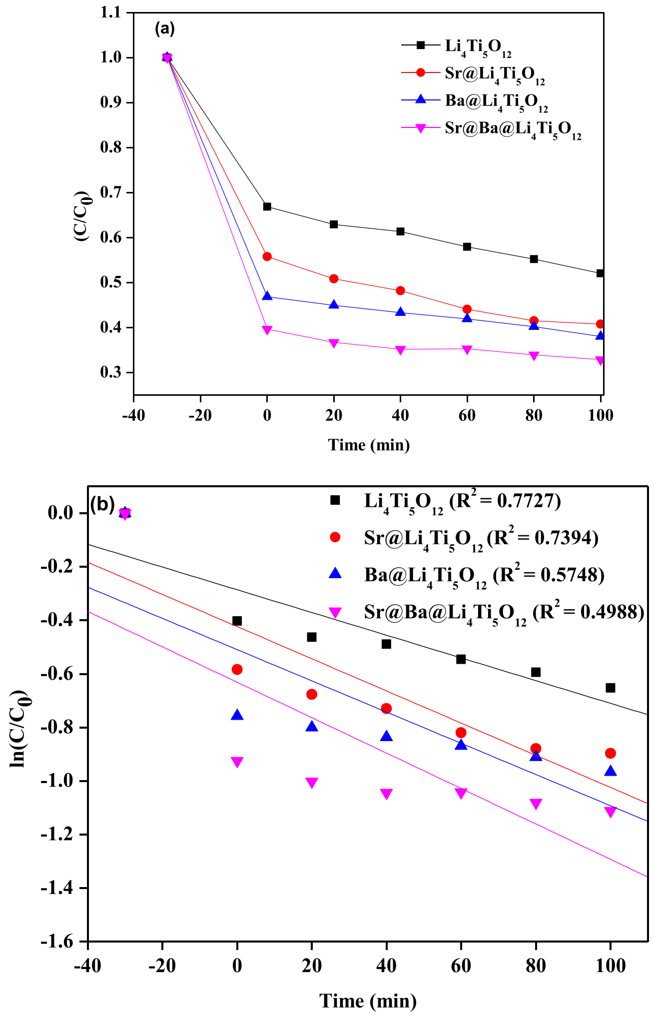

Fig. 8. (a) Degradation of the $Li_4Ti_5O_{12}$ and Sr, Ba, Sr/Ba doped $Li_4Ti_5O_{12}$ samples (b) Pseudo-first-order kinetic plot for MB dye using $Li_4Ti_5O_{12}$ and Sr, Ba, Sr/Ba doped $Li_4Ti_5O_{12}$ samples.

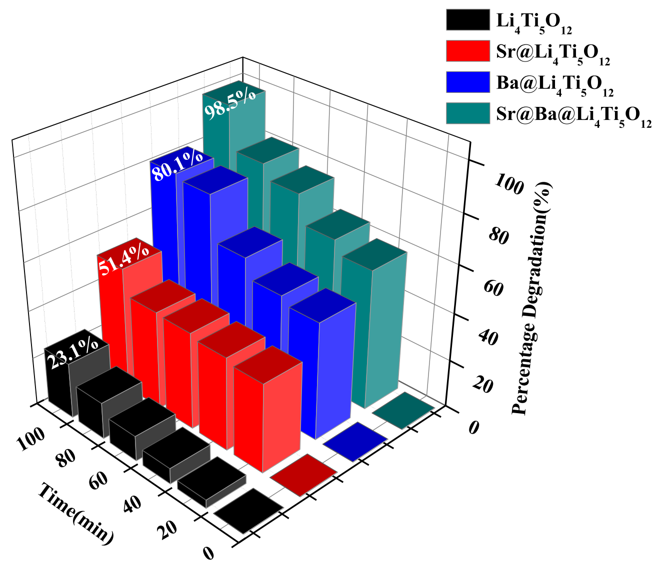

Fig. 9. Degradation efficiency of $Li_4Ti_5O_{12}$ and Sr, Ba, Sr/Ba doped $Li_4Ti_5O_{12}$ samples.

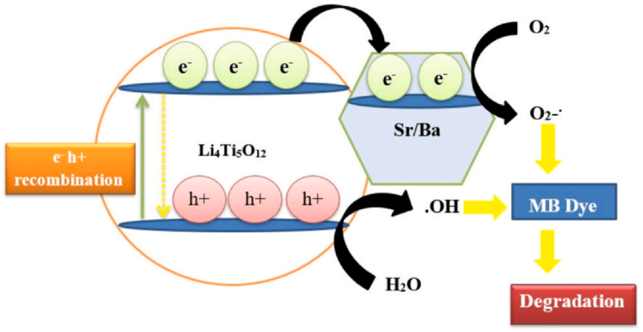

Fig. 10. Decolorization mechanism of Sr/Ba/ $Li_4Ti_5O_{12}$ NPs.

the valence band (VB). This process is known as the photo-excitation reaction. An increase in oxygen vacancies, which serve as active sites for O_2 molecules to adsorb on the photocatalyst surface's conduction band and operate as a potent oxidant without directly contributing to the reduction process, led to an increase in the quantity of superoxide anion free radicals (O.$^{-}$). Furthermore, by interacting with a proton, these superoxide radicals are neutralized, and powerful oxidizing OH^{-} and $OH^{\bullet}$ radicals are produced. By interacting with the dye molecules and converting them into innocuous substances (H_2O, CO_2, NO_2^{-}, NO_3^{-}, etc.), these generated active radicals immediately contribute to degradation [26].

To assess the reuse capability of prepared $Li_4Ti_5O_{12}$ and Sr, Ba, Sr/Ba doped $Li_4Ti_5O_{12}$ samples, four cycles of UV photodegradation for MB dye subtraction were performed. Sr/Ba doped $Li_4Ti_5O_{12}$ NPs maintained their excellent clearance effectiveness (98.5–97 %) throughout four consecutive cycles. over these cycles for MB dye degradation shown in Fig. 11. In Fig. 11, y axis %Z represents the degradation percentage. After the first and second cycles, the degrading efficiency of the Sr/$Li_4Ti_5O_{12}$ photocatalyst for MB dropped to 80.1–79.8 %. The decline in photocatalytic effectiveness of both samples might be ascribed to a diversity of factors, with the reduction of the catalyst's active site as a result of prolonged exposure of $Li_4Ti_5O_{12}$ and Sr, Ba, Sr/Ba doped $Li_4Ti_5O_{12}$ samples to the dye [27]. Additionally, dye molecules continuously absorb light from the catalyst's surface, resulting in a decrease in electron-hole pair formation rates and photodegradation efficiency. Its volume decreases and its photodegradation efficiency decreases when it has been washed and centrifuged. Even after multiple cycles, $Li_4Ti_5O_{12}$ photocatalytic effectiveness remains very stable, allowing it to be reused. Fig. 12 depicts the XRD pattern of the repeated sample. During the cyclic activity, $Li_4Ti_5O_{12}$ and Sr, Ba, Sr/Ba doped

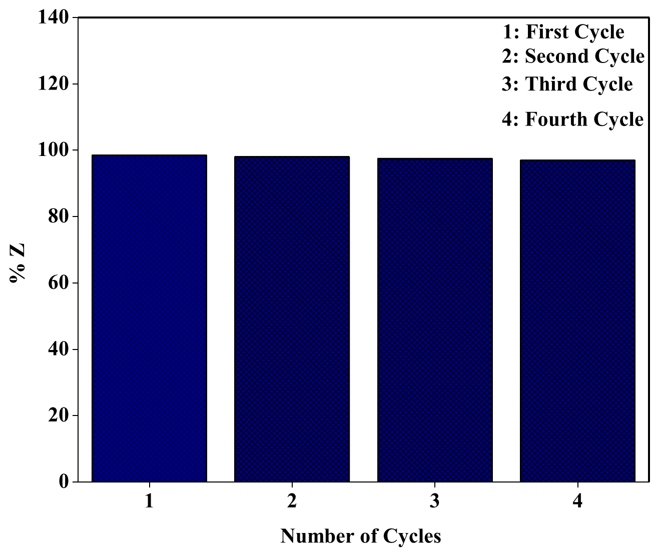

Fig. 11. Reusability examination of Sr/Ba doped $Li_4Ti_5O_{12}$ samples.

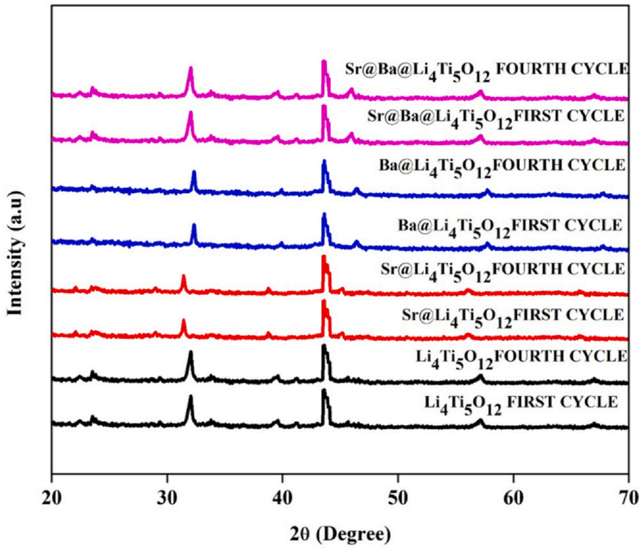

Fig. 12. XRD patterns of prepared $Li_4Ti_5O_{12}$ and Sr, Ba, Sr/Ba doped $Li_4Ti_5O_{12}$ samples before and After four Cycles.

$Li_4Ti_5O_{12}$ samples showed no changes in phase or structure, demonstrating that it is very stable during degradation [28].

4. Conclusion

In conclusion, a two-step method has been effectively used to synthesize a variety of $Li_4Ti_5O_{12}$ and Sr, Ba, and Sr/Ba doped $Li_4Ti_5O_{12}$ nano photocatalysts, which have been used for the photocatalytic destruction of common organic pollutants including MB. The mean size of the particles is between 19 and 26 nm for crystallites. A significant increase in photocatalytic effectiveness was noted upon loading Sr, Ba, and Sr/Ba onto $Li_4Ti_5O_{12}$ surfaces. Both photostability and practicability are excellent for the ideal Sr/Ba loading. The homogeneous dispersion of Sr/Ba/ $Li_4Ti_5O_{12}$ NPs and the increased surface oxygen vacancies on the surfaces of these nanoparticles are the sources of improved photocatalytic effectiveness. Strong interactions between surface oxygen vacancies and Sr, Ba and $Li_4Ti_5O_{12}$ can increase the absorption of UV–vis light and facilitate the separation of photogenerated electrons and holes, leading to an increase in ROS (OH and O_2^{-}) generation. Consequently, the $Li_4Ti_5O_{12}$ NPs is a promising option for treating industrial wastewater in order to get rid of organic contaminants, which pose a serious risk to the environment.

Credit author statement

Dr. K. M. Gopalakrishnan, S. Nilesh, G. Kathiresan, Abhay Kumar, and K. Vallarasu synthesized the materials and also analyzed the data for characterizations. Writing, review, and editing, as well as visualization, were assisted by Dr. V. Vijayalakshmi and R. Anitha. Every author contributed equally to make sure the data were finalized and the manuscript was submitted.

Disclosure of competitive interest

Each of them swears they have no conflicting interests. They further state that this material has never been published before and that no other journal is considering it.

Data Availability

No data was used for the research described in the article.

Declaration of Competing Interest

The authors declare that they have no known competing financial interests or personal relationships that could have appeared to influence the work reported in this paper.

References

[1] Oladoye Peter Olusakin, Ajiboye Timothy Oladiran, Omotola Elizabeth Oyinkansola, Oyewola Olusola Joel. Results Eng 2022;16:100678.
[2] Kim Min Gu, Lee Ji Eun, Kim Kang Seok, Kang Jeong Min, Lee Jeong Hoon, Kim Kwang Ho, Cho Min, Lee Seung Geol. N J Chem 2021;45:3485–97.
[3] Anand Bhaskar, Szulejko Jan E, Kim Ki-Hyun, Younis Sherif A. Environ Pollut 2021;285:117491.
[4] Jayachandran Ashwini, Aswathy TR, Nair Achuthsankar S. Biochem Biophys Rep 2021;26:100995.
[5] Fouladi-Fard Reza, Aali Rahim, Mohammadi- Aghdam Sarvin, Mortazavi-derazkola Sobhan. Arab J Chem 2022;15(3):103658.
[6] MuthuKathija M, Sheik Muhideen Badhusha M, Rama V. Appl Surf Sci Adv 2023;15:100400.
[7] Senthilkumar G, Sakthivelu A, Abdur Rahman M, Parameswari P. Inorg Chem Commun 2023;155:111081.
[8] Mohan NS, Gokulkumar R, Shankar J, Sridharan R, Logesh B, et al. Results Chem 2022;4:100626.
[9] Latif Misbah, Aziz Muhammad Hammad, Shaheen Fozia, Ali Syed Mansoor, Huang Qing. Mater Lett 2024;360:135756.
[10] V. Vijayalakshmi, P. Dhanasekaran, N.M. Ganesan, Molecular Crystals and Liquid Crystals 664 (1), 241–250.
[11] Chun-Ming Liu, Li-Mei Fang, Xiao-Tao Zu, Wei-Lie Zhou. The influence of nickel dopant on the microstructure and optical properties of SnO_2 nano-powders. Chin Phys 2007;16:95.
[12] Zhao B, Ran R, Liu M, Shao Z. Mater Sci Eng R Rep 2015;98:1–71.
[13] Chen J, Yang L, Fang S, Tang Y. Electrochim Acta 2010;55:6596–600.
[14] Vikram Babu B, Vijaya Babu K, Tewodros Aregai G, Seeta Devi L, Madhavi Latha B, Sushma Reddi M, Samatha K, Veeraiah V. Results Phys 2018;9:284–9.
[15] Mohan NS, Pandian M, Vijayalakshmi V. Iran J Chem Chem Eng 2023. DOI NO: 10.30492/IJCCE.2023.2003604.6053.
[16] Song J, Bin H, Zhu C, Zhu S, Pan H, Li Y, Bokhari SW, Zhang D. J Mater Sci: Mater Electron 2018;29(14).
[17] Li M, Zhang H, Liu Z, Su Y, Du C. Chem Eng J 2022;450:138147.
[18] Huang X, Lei R, Yuan J, Gao F, Jiang C, Feng W, Zhuang J, Liu P. Appl Catal B: Environ 2021;282:119586.
[19] Suzuki S, Matsumoto H, Iwase A, Kudo A. Chem Commun 2018;54(75):10606–9.
[20] De Gonçalves RF, de Moura AP, Godinho MJ, et al. Ceram Int 2015;41:3549–54.
[21] Zhou X, Wu S, Li C, Yan F, Bai H, Shen B, Zeng H, Zhai J. Nano Energy 2019;66:104127.
[22] Han C, et al. J Solgel Sci Technol 2017;81:806–13.
[23] Kenchappa Somashekharappa K, Lokesh SV. ACS Omega 2021;6:7248–56.
[24] Chennimalai M, Vijayalakshmi V, Senthil TS, Sivakumar N. Mater Today: Proc 2021;47:1842–6.
[25] Freire JD, Katiyar RS. Lattice dynamics of crystals with tetragonal $BaTiO_3$ structure. Phys Rev B 1988;37:2074–85.
[26] Khan ME, Mohammad A, Ali W, Khan AU, Hazmi W, Zakri W, Yoon T. J Clean Prod 2022;349:131249.
[27] Mohan NS, Bhuvaneswari S, Anitha R, Vijayalakshmi V. Environ Nanotechnol, Monit Manag 2024;21:100922.
[28] Kitchamsetti N, Didwal PN, Mulani SR, Patil MS, Devan RS. Heliyon 2021;7. e07297-e07305.